Effect of Zn interlayer on brazeability of AZ31B–Mg alloy to steel sheet

A. M. Nasiri* and Y. Zhou

The brazeability of AZ31B–H24 magnesium alloy sheet to Zn electroplated, plain carbon steel sheet using an Mg–Al–Zn alloy filler metal and a diode laser heat source has been investigated. While the Zn coating promoted good wetting between the molten filler alloy and the steel sheet, it did not play a direct role in forming the final bond. Bonding between the magnesium alloy and the steel was facilitated by the formation of two transition layers. First, a nanoscale layer of $FeAl_3$ phase formed on the surface of the steel by diffusion of Al from the Mg–Al–Zn brazing alloy into the steel. Upon further cooling, nucleation and growth of either α-Mg + MgZn eutectic phases or $Mg_2(Al,Zn)_3$ phase occurred on the $FeAl_3$ surface layer.

Keywords: Laser brazing, AZ31B Mg sheet, Zn coated steel sheet, Microstructure

Introduction

The ability to effectively join magnesium alloys to steel will facilitate increased application and use of Mg alloys in the automotive and aerospace industries, where joining Mg alloys to steel in order to achieve lightweight, versatile and tailored properties in one composite part is highly desirable. Challenges associated with joining of steels to Mg alloys need to be resolved before its real practical application in industry.

It is difficult to join magnesium alloys directly to steel by conventional fusion welding technologies due to the large difference in their melting temperatures and the nearly zero solubility of magnesium and iron.[1] There is also clear evidence that magnesium and steel do not react with each other.[1] Thus, metallurgical bonding between these two metals will be possible provided another element that can interact and bond with both of them can be applied between the Mg and Fe as an intermediate interlayer element or alloy.

Hybrid laser arc welding,[1–4] friction stir welding[5,6] and resistance spot welding[7] have been examined to joint different grades of steel sheets to Mg alloys. In these studies, various interlayers, such as Al–12Si,[8] Ni,[2,9] Cu,[4] Sn[10] and Zn,[11–13] have been applied between steel and magnesium. Zhao *et al.*[3] used a hybrid laser gas tungsten arc welding process to joint 304 stainless steel to AZ31B magnesium alloy. However, poor tensile strength of the joints was reportedly caused by oxides that formed at the steel/Mg alloy interface. Liu *et al.*[2,4] investigated the effects of Ni and Cu interlayers between steel and AZ31B Mg alloy using the same joining process. These interlayers were found to facilitate the metallurgical bonding between steel and Mg alloy.

Centre for Advanced Materials Joining, University of Waterloo, Waterloo, ON N2L 3G1, Canada

*Corresponding author, email amnasiri@uwaterloo.ca

A diode laser brazing process for joining AZ31B Mg alloy sheet to coated steel sheet was developed in our previous studies,[8–10] where the Al–12Si, Ni and Sn served as the interlayers. All these interlayers were found to facilitate wetting and bonding between Mg alloy and steel sheet. In the case of Al–12Si and Ni interlayers, interlayer elements directly contributed to the final bonding by playing the role of a major alloying element in the interfacial reaction product, e.g. $FeAl_3$ and Fe(Ni) respectively, which were responsible for metallurgical bonding of steel to Mg alloy. In comparison, when Sn interlayer was used between Mg–Al–Zn brazing alloy to steel, the wetting and bonding were facilitated by formation of nanoscale layers of Fe(Al) solid solution followed by $Al_8(Mn,Fe)_5$ on the steel surface. As a result, Sn interlayer did not play a role in creating the final bond. Instead, its primary function was to prevent contamination and oxidation of the steel surface before activation of the flux until molten Mg–Al–Zn brazing alloy can come into direct contact with the steel surface.[10]

Comparing the physical properties of these interlayers shows that Sn has significantly lower melting point temperature than that of the Al–Si and Ni interlayers. The particular role of the Sn interlayer possibly comes from its low melting point temperature. To further study and confirm this behaviour of the interlayer element, another low melting point temperature interlayer element (Zn) was used between steel and Mg alloy in current study. Zn was previously applied between steel and Mg alloy. Liu *et al.*[7] used resistance spot welding to join AZ31B magnesium alloy to DP600 Zn coated steel. They found that a pre-existing transition layer of Fe_2Al_5 between the Zn coating and the steel improved wetting and bonding between the steel and the magnesium alloy. More recently, Tan *et al.*[11–13] have explored the use of Zn interlayer between DP steel and AZ31B alloy during laser welding–brazing process. The similarity between Liu's and Tan's work was that they both used galvanised steel sheet, meaning a layer of Fe–Al intermetallic

Published by Maney on behalf of the Institute
Received 10 September 2014; accepted 8 November 2014
DOI 10.1179/1362171814Y.0000000264

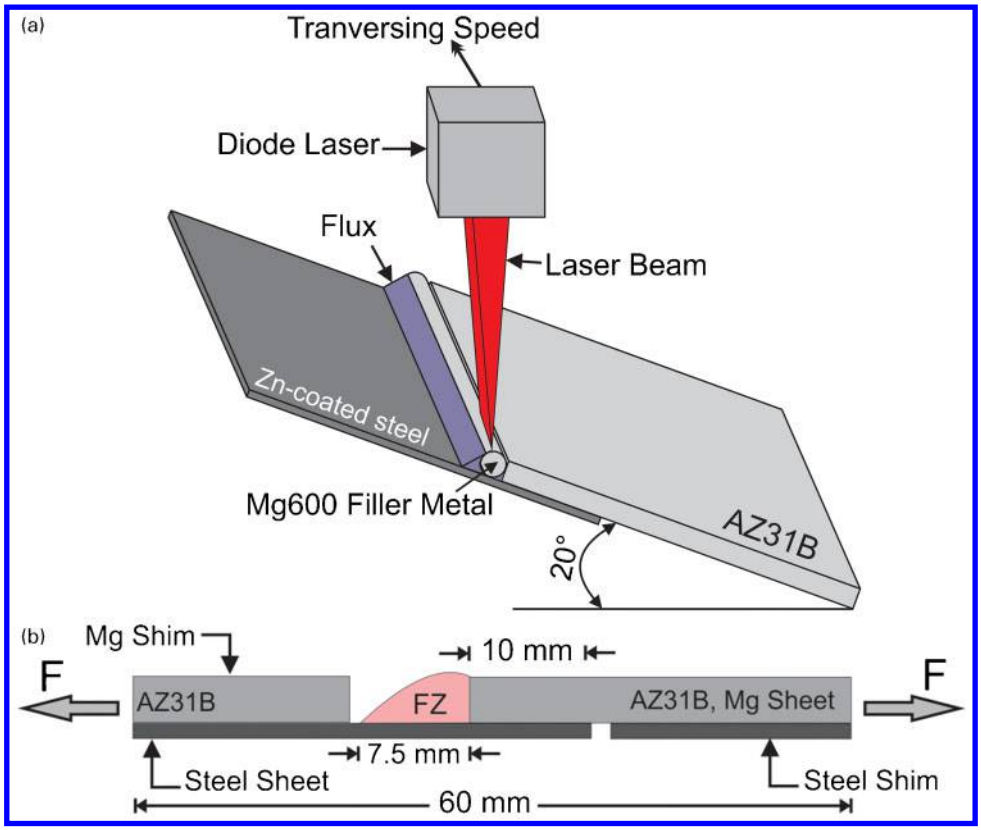

1 ***a*** **schematic of laser brazing system used for joining AZ31B Mg and Zn electroplated steel sheets in lap joint configuration and** ***b*** **schematic of 5 mm wide tensile shear test specimen**

compound (IMC) pre-existed between steel sheet and Zn coating layer, which in both studies was reported to be responsible for metallurgical bonding between steel and magnesium. The available literature does not show the effect of the pure Zn interlayer on the brazeability of the steel to the Mg alloy. Therefore, in this study, diode laser brazing of Zn electroplated steel sheet (with no pre-existing Fe–Al IMC) to AZ31B Mg alloy sheet using Mg–Al–Zn filler metal was investigated.

Experimental

The laser brazing process was carried out on 60×50 mm specimens sheared from 0·8 mm thick Zn electroplated, cold rolled AISI 1008 plain carbon steel sheet and 2 mm thick commercial grade twin roll strip cast AZ31B–H24 Mg alloy sheet. The Zn coating layer on the steel sheet was $2{\cdot}6 \pm 0{\cdot}5$ μm thick. Energy dispersive spectroscopy (EDS) analysis of the Zn layer showed a pure Zn coating layer with no pre-existing Fe–Al IMC at the Zn/steel interface. Tables 1 and 2 show the chemical compositions of the base materials. TiBraze Mg 600 filler wire (Mg–9 wt-%Al–2 wt-%Zn) with 2·4 mm diameter and solidus and liquidus temperatures of 445 and 600°C respectively was used for this study. A powder flux composed of 35–40 wt-%LiCl, 30–35 wt-%KCl, 10–25 wt-%NaF, 8–13 wt-%NaCl and 6–10 wt-%$ZnCl_2$ (commercially named as Superior No. 21[14]) was also used in the experiments.

To remove oil and other contaminants for the specimens' surfaces, all of the specimens were ultrasonically cleaned in acetone. In order to clean the oxide layers on the surfaces of the magnesium sheets, stainless steel wire brushing was used before the laser brazing process. Then, the lab joint configuration was made by clamping the AZ31B Mg alloy sheet on top of the steel sheet. The schematic of the lap joint configuration used in this study is shown in Fig. 1*a*. The filler wire was preset along the joint line with flux before the brazing process.

An integrated Panasonic six-axis robot and Nuvonyx diode laser system with a maximum power of 4·0 kW and a $0{\cdot}5 \times 12$ mm rectangular laser beam intensity profile at the focal point was used for laser brazing. The flux provided enough shielding during the test; therefore, a shielding gas was not necessary. Laser power, laser speed and the beam offset to the steel side were the main parameters of the laser brazing process.

After laser brazing, to measure the mechanical performance of the joints, 5 mm wide rectangular shaped specimens were made from the joints and subjected to tensile shear tests with a crosshead speed

Table 1 Measured chemical composition of AZ31–H24 Mg alloy sheet and TiBraze Mg 600 filler metal/wt-%

	Al	Zn	Mn	Si	Mg
AZ31B–H24	3·02	0·80	0·30	0·01	Bal.
TiBraze Mg 600	9·05	1·80	0·18	…	Bal.

Table 2 Measured chemical composition of 0·8 mm thick steel sheet/wt-%

C	Mn	P	S	Fe
0·01	0·5	0·010	0·005	Bal.

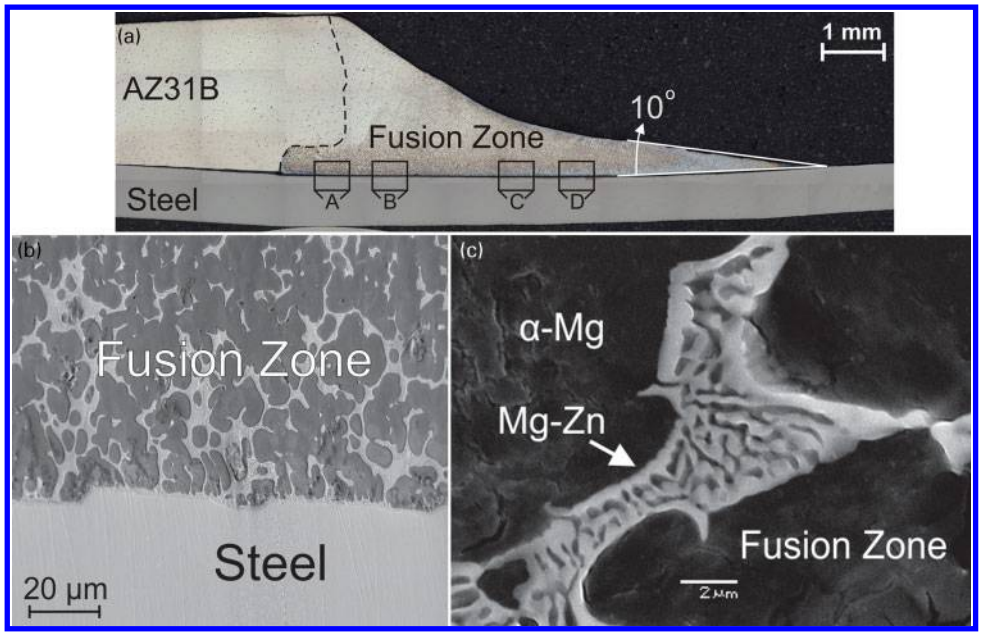

2 ***a*** **optical micrograph of transverse section of laser brazed joint, SEM images of** ***b*** **steel/FZ interface and** ***c*** **lamellar phases formed in FZ**

of 1 mm min^{-1}. Figure 1*b* shows schematic of the tensile shear specimen. To ensure shear loads in the lap joint while minimising induced couples or bending of the specimens, shims were used at each end of the specimens.

Transverse sections of the brazed specimens were cut and mounted in epoxy resin. Standard grinding and polishing sample preparation procedure were performed on the samples for microstructural analyses. The polished specimens were etched by 20 mL acetic acid, 3 g picric acid, 50 mL ethanol and 20 mL water[15] to reveal the microstructure of the braze metal and AZ31B base material.

The microstructure and composition of different zones of the joint cross-section were analysed using a JEOL JSM-6460 SEM equipped with an Oxford INCA energy dispersive X-ray spectrometer. A TEM foil of the steel fusion zone (FZ) interfacial region was also prepared using a focused ion beam and *in situ* lift out technique. After attaching the TEM foil to a copper grid, final Ga^{+} beam thinning was performed on the sample using an acceleration voltage of 30 kV, followed

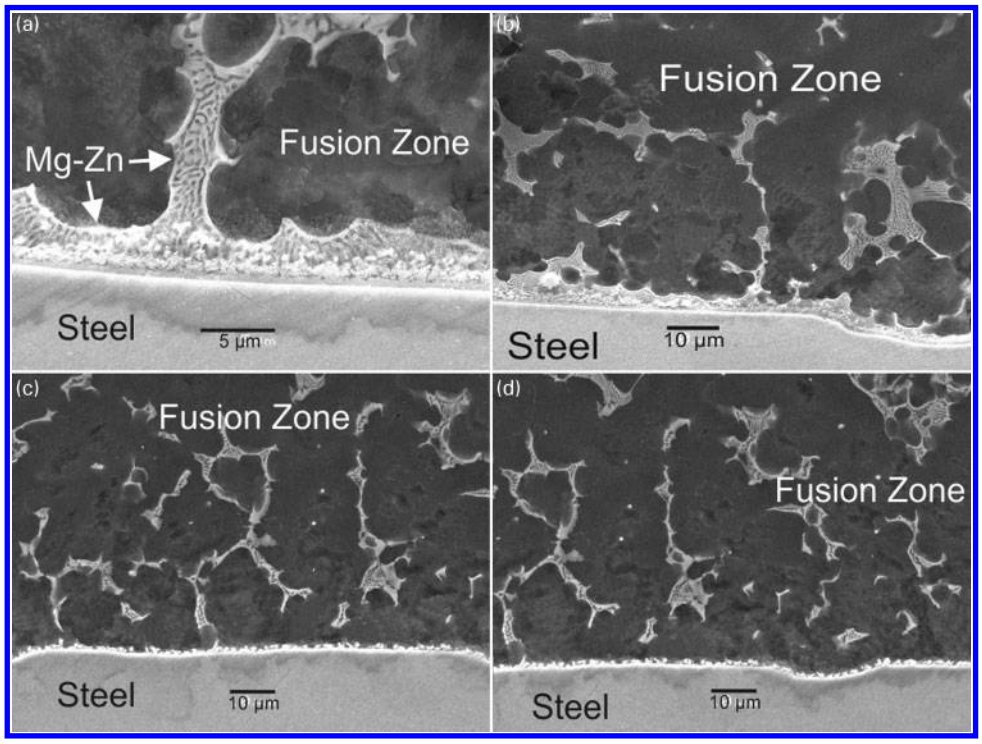

a position A; *b* position B; *c* position C; *d* position D

3 Images (SEM) in different positions (shown in Fig. 2*a*: A–D) along the steel/FZ interface

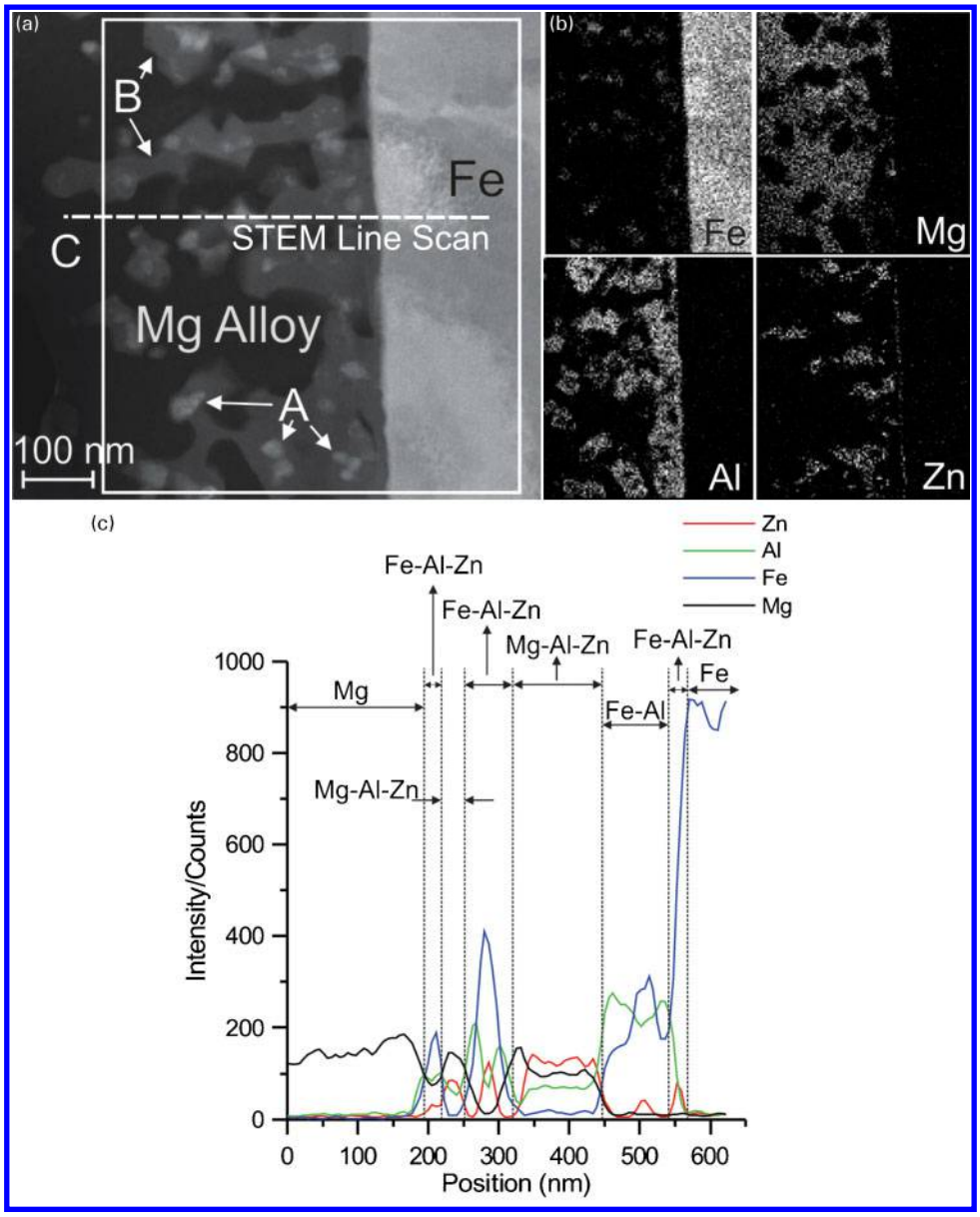

4 ***a*** **image (STEM) of steel/FZ interface from postion C in Fig. 2*a*, *b* STEM-EDS concentration maps of selected square area in *a* and *c* STEM-EDS composition line scans across steel/FZ interface shown in *a*, indicating scans of Mg, Fe, Al and Zn**

by 10, and 1 kV for the final polishing step to get a 100 nm thick TEM sample. The TEM studies were performed using a Titan 80-300LB, a high resolution high resolution TEM/scanning transmission electron microscopy (STEM) made by FEI Company.

Results and discussion

Figure 2*a* shows a cross-sectional overview of a laser brazed Zn electroplated steel sheet–AZ31B Mg sheet specimen. Using 2·2 kW laser power, 8 mm s^{-1} travel speed and 0·2 mm beam offset to the steel side resulted in formation of a visually acceptable fillet with triangular cross-section between the AZ31B Mg and steel base metals. A uniform brazed area with good wetting of filler metal on both base materials and some partial melting of the AZ31B Mg alloy was observed. The average contact angle of the Mg–Al–Zn FZ on the steel substrate was measured to be $10^\circ \pm 3^\circ$, indicative of good wettability of the Zn electroplated steel by molten Mg–Al–Zn alloy.[16] No porosity or crack was observed in the joint.

Microstructural analysis of steel/FZ Interface

Figure 2*b* shows a SEM photomicrograph of the FZ microstructure. The solidification microstructure of the FZ was a combination of columnar and equiaxed α-Mg dendrites with a divorced eutectic β-$Mg_{17}Al_{12}$ intermetallic phase at the dendrite boundaries. More detailed microstructural analysis of the FZ and AZ31B Mg alloy microstructure has been documented in Ref. 8. The Zn coating layer was not detected as a separate layer on the steel along the interface after the laser brazing process. Therefore, the low melting point Zn (T_{mp}=420°C) layer had been entirely melted and dissolved into the molten Mg–Al–Zn filler metal. In the FZ, heavily nucleation of a lamellar phase at the α-Mg dendrite boundaries was detected. Figure 2*c* shows SEM image of this lamellar phase at higher magnification. According to EDS analysis, the dark lamellae corresponded to α-Mg, and

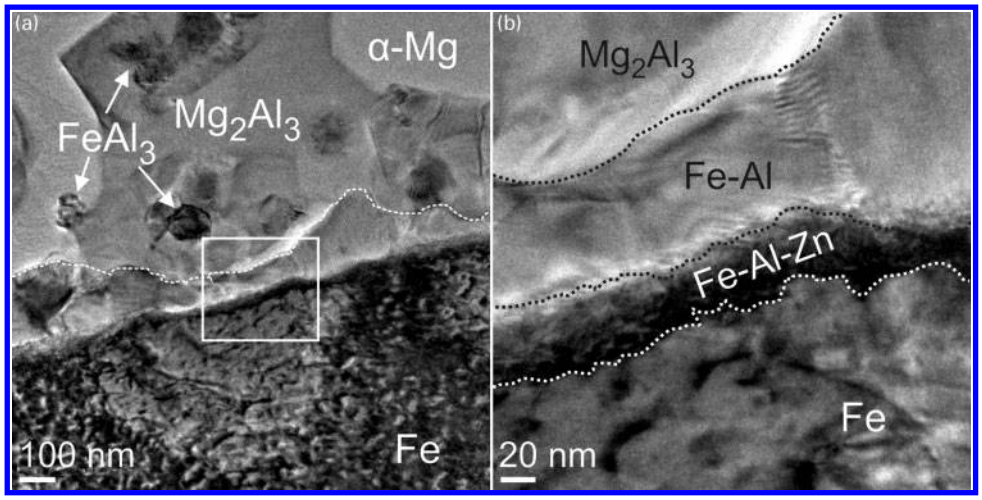

5 Bright field TEM image of *a* Fe/FZ interface and *b* selected square area in *a* in higher magnification

the white lamellae containing 46·4±6·4 wt-%Mg, 45·5±3·4 wt-%Zn and 8·1±1·3 wt-%Al represented the MgZn stoichiometric IMC. This was confirmed by selected area diffraction pattern (SADP) analysis results presented later in the following sections. These two phases next to each other are the α-Mg+MgZn lamellar eutectic. MgZn phase was mainly precipitated in the FZ adjacent to the steel surface. Formation of MgZn even far from the steel surface in the FZ confirmed diffusion of Zn atoms into Mg alloy filler metal. Therefore, the laser brazing temperature and duration were high enough for entire Zn coating to melt and diffuse into the Mg alloy and as a result high volume fraction of MgZn phase precipitates in the FZ. The MgZn eutectic phase is well known for its brittle nature and low fracture toughness.[17] Therefore, formation of this phase in the laser brazed joint is harmful for mechanical performance of the joints.

Figure 3 shows microstructure at different positions of the steel/FZ interface from the root to the head of the laser brazed joint, labelled from A to D in Fig. 2*a*. It was observed that microstructure of the steel/FZ interface changed significantly across the interface from the root (Fig. 3*a*, position A) to the head (Fig. 3*d*, position D) of the joint. At the root of the interface, a continuous layer of lamellar MgZn eutectic formed on the steel surface (Fig. 3*a*). This phase was nucleated and grown as a continuous layer over the interface from the root (position A) to halfway through the brazed length (between positions B and C).

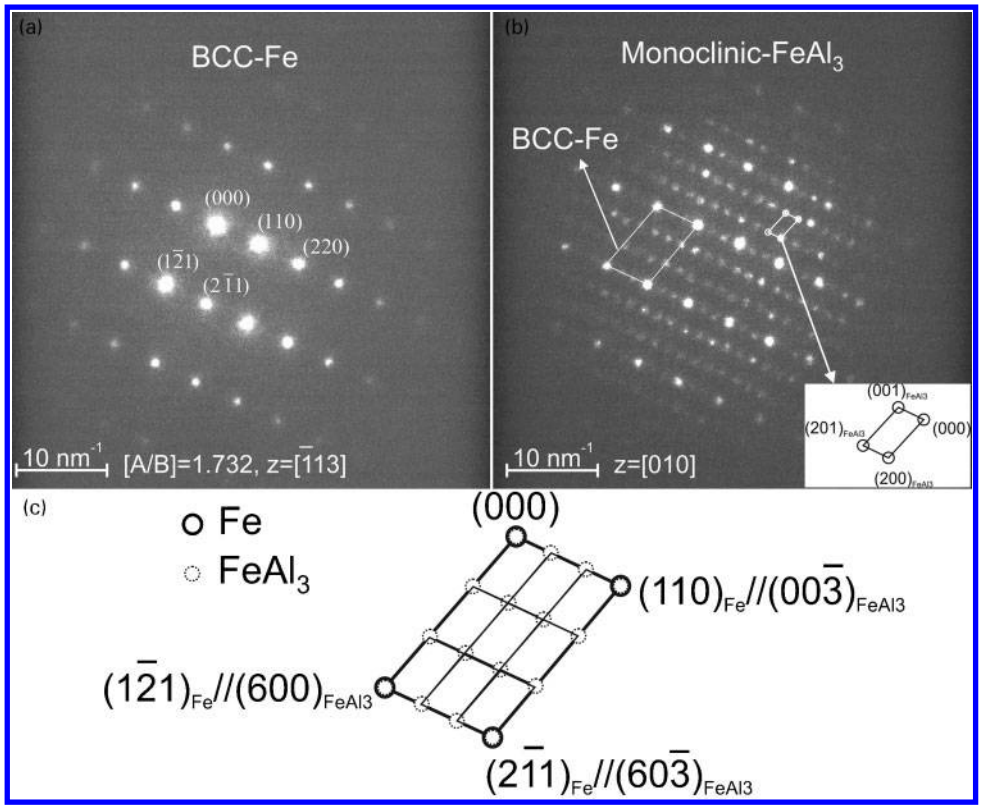

6 *a* selected area diffraction pattern of Fe in [$\bar{1}$13] zone axis of phase, *b* corresponding SADP of Fe/$FeAl_3$ interface and *c* schematic representing orientation relationship (OR) between Fe and $FeAl_3$

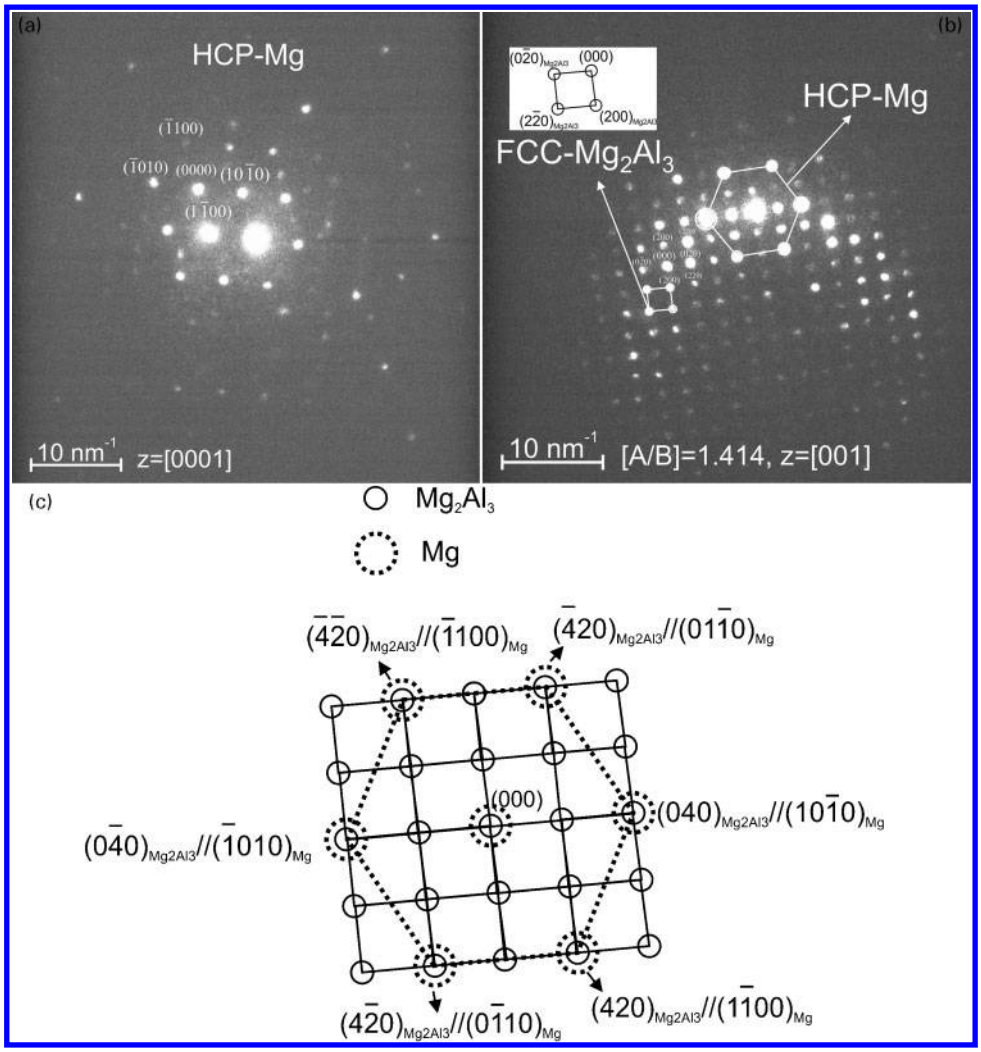

7 ***a*** **selected area diffraction pattern of Mg in [0001] zone axis of phase,** ***b*** **corresponding SADP of Mg/Mg_2Al_3 interface and** ***c*** **schematic representing OR between Mg and Mg_2Al_3**

Upon moving from position B to position C, the morphology of the interfacial phase changed from the continuous MgZn layer to a dendritic shaped phase (*see* Fig. 3*c*). From position C to the head of the joint, this dendritic phase was nucleated and grown on the steel surface.

In order to identify the dendritic phase together with any other possible formed phase(s) at the steel/FZ interface, TEM analysis of the interface was performed in position C. Figure 4 shows a STEM image of the steel/FZ interface. The dendritic phase appeared as the light grey phase on the steel surface, as shown in Fig. 4*a* (denoted as B). In addition, some white particle-like phases (denoted as A) were found in the FZ adjacent to the interface. According to the STEM-EDS point analysis results, phases B and A contained $40{\cdot}4\pm1{\cdot}4$ at-%Mg, $58{\cdot}2\pm1{\cdot}4$ at-%Al, $1{\cdot}3\pm0{\cdot}1$ at-%Zn and $83{\cdot}6\pm3{\cdot}7$ at-%Al, $12{\cdot}9\pm4{\cdot}3$ at-%Fe, $3{\cdot}5\pm1{\cdot}7$ at-%Zn respectively. The SADP analyses confirmed that dendritic phase (phase B) corresponded to $Mg_2(Al,Zn)_3$ with face centred cubic crystal structure and white particles (phase A) are $Fe(Al,Zn)_3$ with monoclinic crystal structure. It has been reported that each of the Mg_2Al_3 and $FeAl_3$ phases have some solubility for substitutional Zn atoms.[18,19]

To further identify the formed phases at the steel/FZ interface, STEM-EDS compositional mapping and line scanning analysis were used. Figure 4*b* shows the concentration maps for Fe, Mg, Al and Zn. Fe is seen to be present not only in the steel side but also in some small regions in the FZ, corresponding to $FeAl_3$ particles. Mg exists in the FZ, but is not present in the steel side. This is consistent with immiscibility of Mg and Fe into each other.[1] There is a significant concentration of Al from the filler metal within the FZ and the interface, mainly corresponding to the $Mg_2(Al,Zn)_3$. Similar to Al with lower concentration, Zn was found to exist not only in the $Mg_2(Al,Zn)_3$ phase but also on the steel surface. The results of the STEM-EDS line scan confirmed high concentration of Al and Zn elements between the $Mg_2(Al,Zn)_3$ phase and the steel surface shown in Fig. 4*c*. The Al concentration on the Fe substrate showed significantly higher intensity than Al of the $Mg_2(Al,Zn)_3$ phase. To further study the source for high Al content on the steel surface, TEM analysis in higher magnification was used. Figure 5 shows a typical bright field TEM image of the steel/FZ interface. The region between $Mg_2(Al,Zn)_3$ phase and steel is shown in higher magnification in Fig. 5*b*. Two nanoscale layers of Fe–Al–Zn and Fe–Al phase were observed to grow on the steel surface. The SADP analysis of this layer indicated that this phase is a $FeAl_3$ IMC. The diffraction pattern was taken along $[010]_{FeAl_3}$ zone axis of the phase

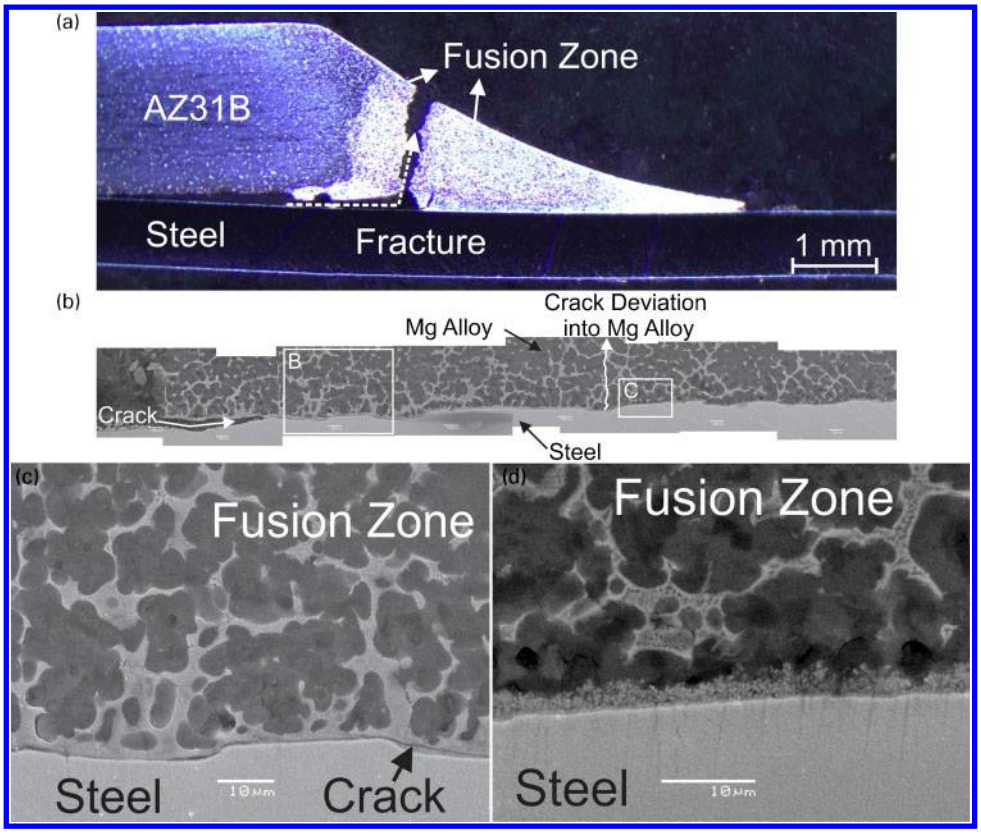

8 ***a*** **typical fractured specimen after tensile shear test of laser brazed joint,** ***b*** **crack propagation path during tensile shear test,** ***c*** **higher magnification of area B, selected square area in** ***b*****, showing cracked MgZn phase at interface and** ***d*** **area C at higher magnification, showing steel/FZ interface where MgZn phase was non-existent at interface**

(*see* Fig. 6*b*). The Fe–Al–Zn phase showed similar diffraction pattern and lattice parameters and corresponded to the $Fe(Al,Zn)_3$. Therefore, the second layer is also $FeAl_3$ with some substitutional Zn atoms. This phase was formed all over the interface on the steel and bonded the steel to the Mg alloy.

Selected area diffraction pattern analysis was performed to analyse OR at $Fe/Fe(Al,Zn)_3$ and $Mg/Mg_2(Al,Zn)_3$ interfaces. To identify the OR between Fe and $Fe(Al,Zn)_3$ at their interface, first the TEM foil was tilted until the incident beam was parallel to the $[\bar{1}13]_{Fe}$ zone axis of the Fe grain, and the SADP shown in Fig. 6*a* was taken from the Fe. Then, without changing the orientation of the beam and specimen with respect to each other, the SADP of the $Fe/Fe(Al,Zn)_3$ interface was taken, as shown in Fig. 6*b*. The results showed that the $Fe(Al,Zn)_3$ phase was located on $[010]_{Fe(Al,Zn)_3}$ zone axis, when Fe was parallel to $[\bar{1}13]_{Fe}$ zone axis. These results imply that $[\bar{1}13]_{Fe}//[010]_{Fe(Al,Zn)_3}$. Furthermore, some diffraction spots from each phase were superimposed with each other. This indicates that the crystallographic plane relationship between the formed $Fe(Al,Zn)_3$ phase at the interface and Fe grain in this site was $(110)_{Fe}//(00\bar{3})_{FeAl_3}$, $(1\bar{2}1)_{Fe}//(600)_{FeAl3}$, and $(2\bar{1}1)_{Fe}//(60\bar{3})_{FeAl3}$. Therefore, the SADP analysis of the Fe and $Fe(Al,Zn)_3$ confirmed the OR between these two phases.

The SADP analysis of the $FeAl_3/Mg_2(Al,Zn)_3$ interface did not show a specific OR between $FeAl_3$ and $Mg_2(Al,Zn)_3$ at their interface. The SADP analysis of the $Mg/Mg_2(Al,Zn)_3$ interface (shown in Fig. 7) confirmed that the OR between the formed $Mg_2(Al,Zn)_3$ and Mg at the interface was $[001]_{Mg2Al3}//[0001]_{Mg}$. The superimposed diffraction spots of these phases at their interface imply that there is a good OR with low angle rotation of matching planes between Mg and $Mg_2(Al,Zn)_3$ at their interface, e.g. $(\bar{4}\bar{2}0)_{Mg2Al3}//(\bar{1}100)_{Mg}$, $(\bar{4}20)_{Mg2Al3}//(01\bar{1}0)_{Mg}$, $(0\bar{4}0)_{Mg2Al3}//(\bar{1}010)_{Mg}$, $(040)_{Mg2Al3}//(10\bar{1}0)_{Mg}$, $(4\bar{2}0)_{Mg2Al3}//(0\bar{1}10)_{Mg}$ and $(420)_{Mg2Al3}//(1\bar{1}00)_{Mg}$.

Fracture behaviour

The average tensile shear strength of the laser brazed Zn electroplated steel–AZ31B Mg joints using Mg–Al–Zn filler metal was $1086{\cdot}4 \pm 150{\cdot}2$ N. This is 41% higher and 47% lower than tensile shear strength of the laser brazed steel–AZ31B Mg alloy, when Al–12Si and Sn were used as the interlayers respectively.[8,10] Figure 8*a* shows a typical fractured laser brazed specimen after tensile shear test. All tensile shear specimens showed a mixed fracture of the FZ and the steel/FZ interface (shown by a dashed arrow on Fig. 8*a*). To understand this mixed fracture behaviour, the crack propagation path was further studied using peak hold tensile test.[20] For this test, the tensile shear testing was stopped immediately after the maximum load was reached. Afterwards, the cracked specimen was examined using SEM to investigate the location of the initiated crack before fracture. This test shows the weakest phase(s) existed in the structure of the joint.

Figure 8*b* shows a typical cracked specimen indicating the crack propagation path before final fracture of the specimen. As shown clearly in Fig. 8b, the crack first

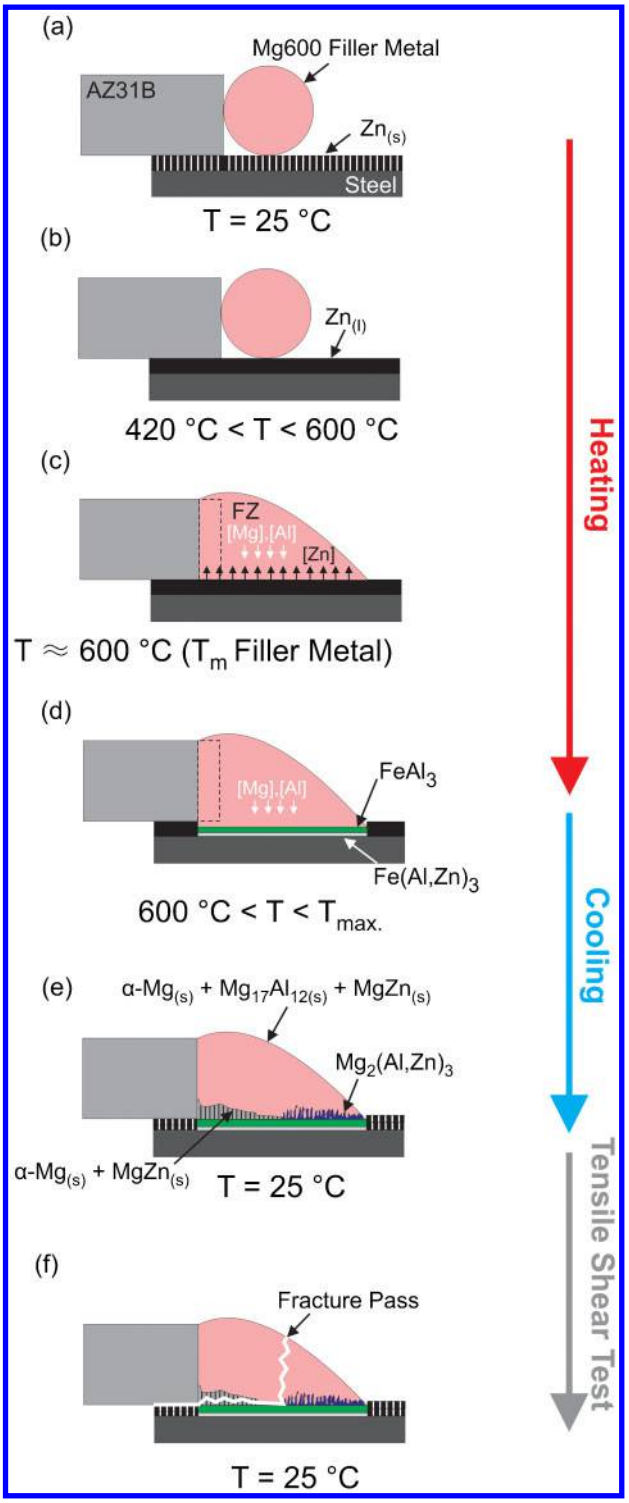

a lab joint design configuration before laser brazing process at room temperature; *b* melting of Zn electroplated layer during heating; *c* melting of filler metal and dissolution of liquid Zn into FZ; *d* formation of $Fe(Al,Zn)_3$ and $FeAl_3$ phases on top of steel substrate; *e* nucleation of $Mg_2(Al,Zn)_3$ and MgZn IMCs on top of $FeAl_3$ phase and solidification of FZ during cooling; *f* fractured specimen after tensile shear test of laser brazed joint

9 Schematic of interfacial layers formation during laser brazing of Zn electroplated steel–AZ31B with Mg alloy filler metal

initiated from the sharp slit between the steel sheet and AZ31B Mg sheet, then propagated in the α-Mg + MgZn eutectic structure along the steel/FZ interface (*see* Fig. 8*c*) and finally deviated into the FZ. The crack deviated from the steel/FZ interface to the FZ, where the MgZn was non-existent at the interface (as shown in Fig. 8*d*). Therefore, the low fracture toughness of MgZn stoichiometric compound dictated the fracture pass and low strength of the laser brazed joint. Dendritic Mg_2Al_3 non-stoichiometric phase at the interface was found to be mechanically resistant to the crack propagation.

Sequence of phase formation along interface (bonding mechanism)

From the above results, for formation of a metallurgical bond between Zn electroplated steel and Mg–Al–Zn filler metal during laser brazing process a sequence of reactions may take place. These are shown in the schematics in Fig. 9 starting with lap joint configuration at room temperature (Fig. 9*a*). The electroplated Zn layer melts during heating stage of the laser brazing when the temperature exceeds the melting point temperature of the Zn (420°C). The $Zn_{(l)}$ still covers the steel surface and prevents it from oxidation and contamination before the activation of the flux (Fig. 9*b*). The flux is activated at 600°C, and then melting of the Mg–Al–Zn filler metal starts. Then, the liquid Zn diffuses from the steel surface into the FZ, thereby allowing direct contact between the molten filler metal and the clean, oxide free steel surface (Fig. 9*c*). Meanwhile, Al atoms from the FZ preferentially diffuse very rapidly from the molten FZ into the steel leading to the formation of a $Fe(Al,Zn)_3$ and $FeAl_3$ IMC layers on the steel. Some Fe atoms from the substrate also diffuse into the FZ adjacent to the interface and resulted in nucleation of particle-like $FeAl_3$ phase in the FZ close to the interface (Fig. 9*d*). As cooling and solidification begin, the newly formed $FeAl_3$ layer plays the role of the new substrate for heterogeneous nucleation and growth of either the Mg_2Al_3 phase or α-Mg + MgZn eutectic phases from the FZ. As temperature continues to drop, solidification of the FZ continues with nucleation of the primary α-Mg and finishes with formation of α-Mg + $Mg_{17}Al_{12}$ eutectic and α-Mg + MgZn eutectic phases in an equiaxed dendritic structure (Fig. 9*e*).

Therefore, bonding between the steel sheet and the Mg–Al–Zn brazing alloy was facilitated by the formation of $FeAl_3$ layer, which was bonded to the steel from one side and to either Mg_2Al_3 or MgZn from its other side. Despite nucleation of the MgZn eutectic phase in the FZ and in some area on the $FeAl_3$ layer, Zn coating did not appear to play a role in creating the final bond between the steel sheet and the Mg–Al–Zn brazing alloy. However, existence of this layer on the steel was necessary to prevent oxidation of the steel surface before the activation of the flux. After melting of the filler metal, dissolution of the Zn into the Mg–Al–Zn filler metal allows a clean and oxide free steel surface to come in direct contact with filler metal. Similar functional behaviour for the interlayer was also observed in our previous study when Sn was used as the interlayer element between steel and AZ31B Mg alloy.[10] The main similarity of these two interlayer elements is their low melting point temperature. In comparison, higher melting point temperature interlayers, such as Al or Ni, were found to directly contribute to the final bonding by playing the role of a major alloying element in the reaction product, e.g.

$FeAl_3$ and Fe(Ni) respectively, which were responsible for metallurgical bonding of steel to Mg alloy.[8,9]

Conclusions

1. Diode laser brazing was performed between 0·8 mm thick Zn electroplated plain carbon steel sheet and 2 mm thick AZ31B–H24 Mg alloy sheet using a Mg–Al–Zn filler metal. Visually acceptable braze joints were produced using 2·2 kW laser beam power moving at 8 mm s^{-1} travel speed along the joint.

2. No evidence of the Zn coating on the steel surface was found after the laser brazing process. Instead, there was a nanoscale layer of $Fe(Al,Zn)_3$. Formation of a thin layer of either α-Mg + MgZn eutectic or $Mg_2(Al,Zn)_3$ was also observed on the surface of $Fe(Al,Zn)_3$ layer.

3. Selected area diffraction pattern analyses of the Fe–$Fe(Al,Zn)_3$ and Mg–$Mg_2(Al,Zn)_3$ interfaces showed that a crystallographic OR with low angle rotation of the matching planes existed at the interfaces.

4. The Zn coating does not appear to contribute to the final bonding of the steel to the Mg–Al–Zn filler alloy.

5. The average tensile shear strength of the laser brazed joints was $1086{\cdot}4 \pm 150{\cdot}2$ N. In all cases, cracks formed in the brittle MgZn eutectic layer at the steel/FZ interface. Cracking then moved into the FZ, where the interfacial MgZn layer was non-existent.

Acknowledgements

The authors wish to acknowledge support of the American Welding Society Graduate Fellowship programme and the Magnesium Network of Canada (MagNET) supported by the Natural Sciences and Engineering Research Council of Canada for sponsoring this work.

References

1. L. Liu: 'Welding and joining of magnesium alloys', 1st edn; 2005, Cambridge, Woodhead Publishing Ltd.
2. L. Liu and X. Qi: 'Strengthening effect of nickel and copper interlayers on hybrid laser-TIG welded between magnesium alloy and mild steel', *Mater. Des.*, 2010, **31**, (8), 3960–3963.
3. X. Zhao, G. Song and L. Liu: 'Microstructure of dissimilar metal joint with magnesium alloy AZ31B and steel 304 for laser-tungsten inert gas lap welding', *Trans. Chin. Weld. Inst.*, 2006, **27**, 56–62.
4. L. M. Liu and X. Qi: 'Effects of copper addition on microstructure and strength of the hybrid laser-TIG welded joints between magnesium alloy and mild steel', *J. Mater. Sci.*, 2009, **44**, 5725–5731.
5. T. Liyange, J. Kilbourne and A. P. Gerlich: 'Joint formation in dissimilar Al alloy/steel and Mg alloy/steel friction stir spot welds', *Sci. Technol. Weld. Joining*, 2009, **14**, (6), 500–508.
6. S. Jana, Y. Hovanski and G. J. Grant: 'Friction stir lap welding of magnesium alloy to steel: a preliminary investigation', *Metall. Mater. Trans. A*, 2010, **41A**, (12), 3173–3182.
7. L. Liu, L. Xiao, J. C. Feng, Y. H. Tian, S. Q. Zhou and Y. Zhou: 'The mechanism of resistance spot welding of magnesium to steel', *Metall. Mater. Trans. A*, 2010, **41A**, (10), 2651–2661.
8. A. M. Nasiri, L. Li, S. H. Kim, Y. Zhou, D. C. Weckman and T. C. Nguyen: 'Microstructure and properties of laser brazed magnesium to coated steel', *Weld. J.*, 2011, **90**, (11), 211s–219s.
9. A. M. Nasiri, D. C. Weckman and Y. Zhou: 'Interfacial microstructure of diode laser brazed AZ31B magnesium to steel sheet using a nickel interlayer', *Weld. J.*, 2013, **92**, (1), 1s–10s.
10. A. M. Nasiri, D. C. Weckman and Y. Zhou: 'The effect of a Sn interlayer on brazebility of AZ31B magnesium to steel sheet', 2014, to be published.
11. C. W. Tan, Y. B. Chen, L. Q. Li and W. Guo: 'Comparative study of microstructure and mechanical properties of laser welded-brazed Mg/steel joints with four different coating surfaces', *Sci. Technol. Weld. Joining*, 2013, **18**, (6), 466–472.
12. L. Li, C. Tan, Y. Chen, W. Guo and C. Mei: 'CO_2 laser welding-brazing characteristics of dissimilar metals AZ31B Mg alloy to Zn coated dual phase steel with Mg based filler', *J. Mater. Process. Technol.*, 2013, **213**, 361–375.
13. L. Li, C. Tan, Y. Chen, W. Guo and F. Song: 'Comparative study of microstructure and mechanical properties of laser welded-brazed Mg/mild steel and Mg/stainless steel joints', *Mater. Des.*, 2013, **43**, 59–65.
14. Material Safety Data Sheet, Flux No. 21, Superior Flux & Mfg. Co., Cleveland, OH, 2003, available at http://www.superiorflux.com/superior_flux_msds_spec_sheets.html.
15. G. F. Vander Voort: 'Metallography principles and practice'; 1999, Materials Park, OH, ASM International.
16. M. M. Schwartz: 'Brazing'; 1987, Materials Park, OH, ASM International.
17. L. Li, C. W. Tan, Y. Chen, W. Guo and X. Hu: 'Influence of Zn coating on interfacial reactions and mechanical properties during laser welding-brazing of Mg to steel', *Metall. Mater. Trans. A*, 2012, **43A**, (12), 4740–4754.
18. W. B. Pearson: 'Lattice spacings and structures of metals and alloys'; 1958, New York, Pergamon Press.
19. P. Perrot, J. C. Tissier and J. Y. Dauphin: 'Stable and metastable equilibria in the Fe-Zn-Al system at 450°C', *Z. Metallkd.*, 1992, **83**, (11), 786–790.
20. S. T. Niknejad, L. Liu, T. Nguyen, M. Y. Lee, S. Esmaeili and Y. Zhou: 'Effects of heat treatment on grain-boundary β-$Mg_{17}Al_{12}$ and fracture properties of resistance spot-welded AZ80 Mg alloy', *Metall. Mater. Trans. A*, 2013, **44A**, (8), 3747–3756.